Proceedings: The 7th International Seminar on Double Layer Capacitors,
Deerfield Beach, FL, U.S.A., December 8–10, 1997.

METAL OXIDE SUPERCAPACITOR FOR AUTOMOTIVE APPLICATIONS

Part I: Replacement of Starter Batteries

P. KURZWEIL, O. SCHMID, A. LÖFFLER

Dornier GmbH, Daimler-Benz Research Dept. F1M/BE, 88039 Friedrichshafen, Germany

---

The DORNIER supercapacitors were developed in the early 1990s, when there was an urgent demand for highly compact capacitors for space applications. At that time, research activities concentrated on delevoping an electric short-time power storage device to supply 40 watts of HF-power for the micro-wave antenna of the European Remote Sensing Satellite (ERS), which was launched to observe global changes in the geosphere and atmosphere [1]. In the mid-90ies the DORNIER research division was reorganized and integrated in the DAIMLER-BENZ group. Since then research has been focusing on improving automotive and railway systems [2].

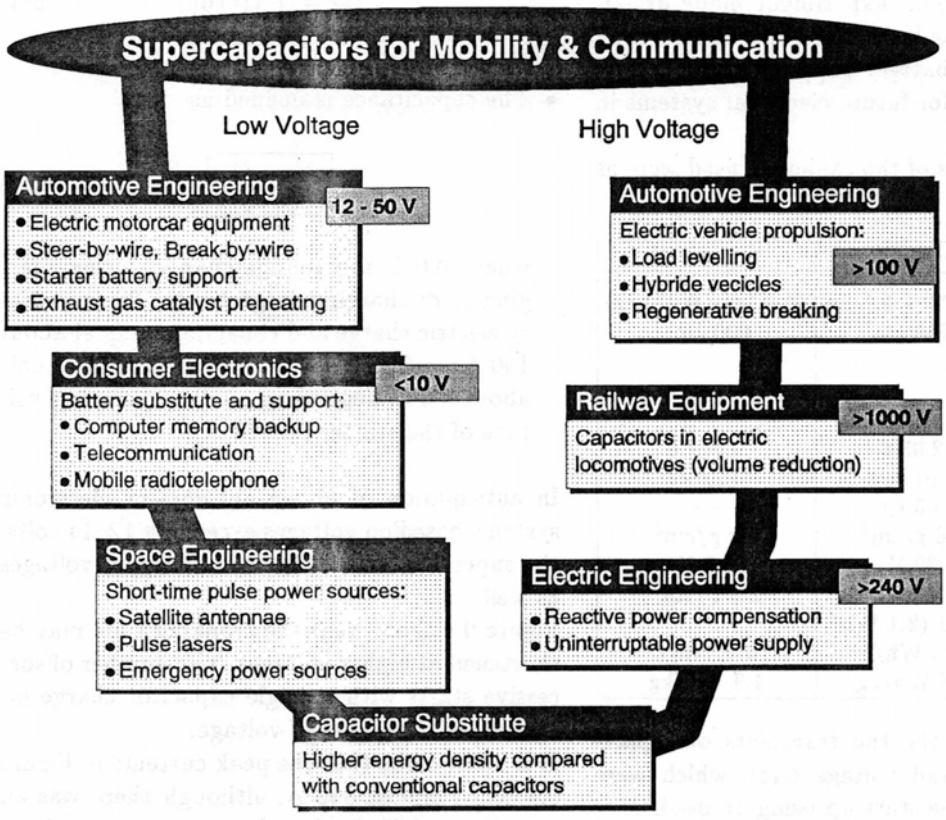

FIGURE 0.1: Potential applications of supercapacitors in different market segments.

Supercapacitors, a spin-off development of space research, have opened up and been integrated into a broad range of mobility and communication technologies (Figure 1).
The DORNIER supercapacitors are based on precious metal oxide hydrates, which have been shown to be highly capacitive and low-resistive materials for electrochemical cells [3, 4, 5, 6].
This paper deals with technical applications of the DORNIER supercapacitors in automotive systems, describes details of the operating behavior, and outlines short-term goals.

STARTING A CAR

In order to demonstrate the impressive power and efficiency of a supercapacitor, we used the 30 V supercapacitor shown in Figure 0.2 to repeatedly start a MERCEDES C220 on a crisp spring morning, at ambient temperatures of 12 °C.
The battery was completly disconnected from the starter, the supercapacitor completely replacing the battery. This experiment made drastically higher demands on the supercacitor than the mere starter battery support, which might be a requirement for future electrical systems in automobiles.
The characteristics of the capacitor used were as follows:

	Total stack	Single cell
Dimensions	33 × 33 × 5.7 cm	30 × 30 × 0.075 cm
Cross-sect. area	1089 cm^2	900 cm^2
Volume		
— total	6.2 ℓ	—
— active	2.03 ℓ	0.068 ℓ
Mass	10 kg	0.22 kg
Endplates	3.5 kg	—
Density	1.6 g/cm^3	3.2 g/cm^3
Voltage	30 V	1.0 V
Capacitance	65 F	2.2 F/cm^2
Th. Energy	29 kJ (8.1 Wh)	
	1.3 Wh/ℓ	4.0 Wh/ℓ
	0.8 Wh/kg	1.3 Wh/kg

Figure 0.3 shows the the transients of capacitor current $I(t)$ and voltage $U(t)$, which were recorded during the start-up using an oscilloscope. The mean values of power and energy were numerically calculated as a function of instanteneous current and voltage.

- The stored or discharged energy during charging or discharging time Δt respectively:

$$\boxed{W = \int_0^{\Delta t} U(t)\, I(t)\, \mathrm{d}t}. \qquad (0\text{-}1)$$

The energy is a function of voltage, temperature and the discharge conditions. The details are outlined in the next section.

- The average electric power during charge or discharge respectively reads:

$$\boxed{\bar{P} = \frac{W}{\Delta t}}. \qquad (0\text{-}2)$$

The actual power demand of the starter and total resistance of capacitor, starter, cables and contacts are shown in Figure 0.3. During cranking an almost constant electric power of about 1 kW was measured.

- The stored or discharged quantity of electricity were determined by integrating the current transient:

$$\boxed{Q = \int_0^{\Delta t} I(t)\, \mathrm{d}t}. \qquad (0\text{-}3)$$

- The capacitance is defined as

$$\boxed{C = \frac{Q}{\Delta U}}, \qquad (0\text{-}4)$$

where ΔU is the voltage change during charging or discharging respectively. The necessary electric charge and capacitance equal about 150 As and 33 F for a single start. ΔU equals about 4.5 V depending on the operating voltage of the starter (12–18 V).

In anticipation of future automotive electronic systems based on voltages exceeding 12–14 volts, the supercapacitor was tested at higher voltages as well.
Figure 0.4 shows that the cranking time may be shortened at higher voltages. The number of successive starts with a single capacitor charge increases as a function of voltage.
It is noteworthy that the peak currents in Figure 0.4 reach almost 300 A, although there was an experimental limitation due to an extraordinary contact resistance between the capacitor and starter, which normally does not occur in the electric system of a car. The short circuit current of the capacitor, however, is in the kiloampere range (see next section).

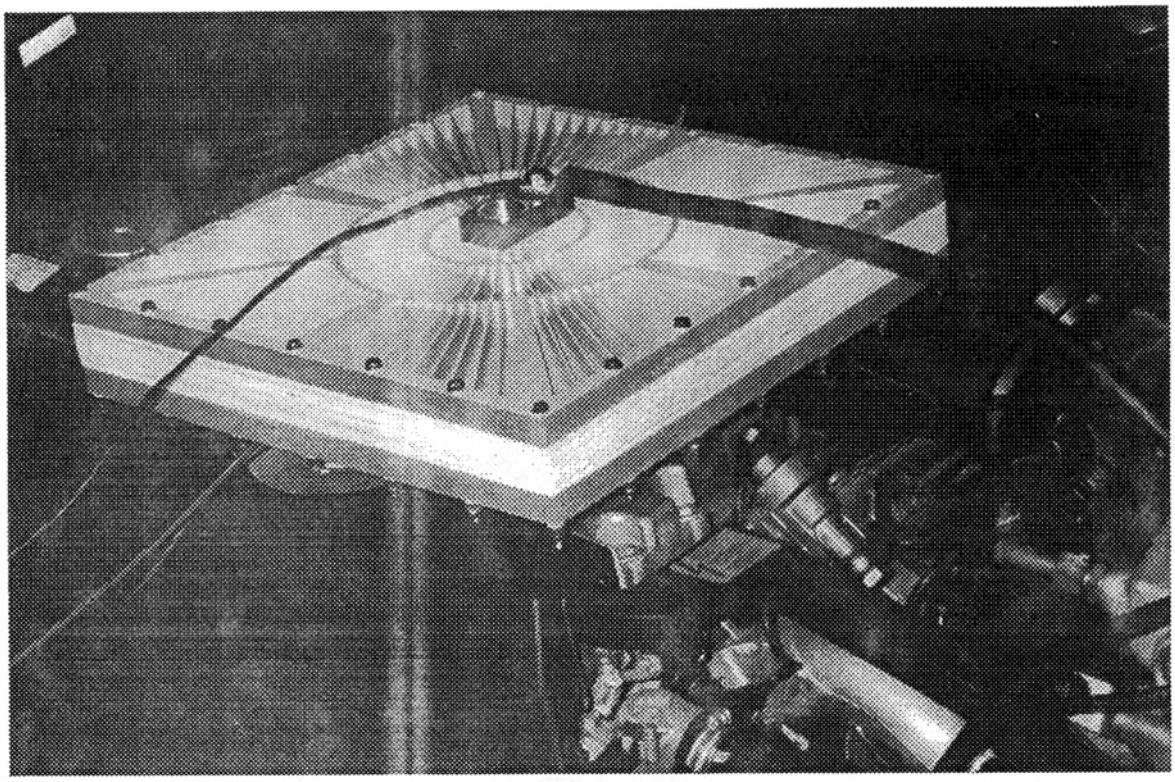

FIGURE 0.2: The DAIMLERBENZ 30 V/65 F-supercapacitor ready for cranking a MERCEDES C220 car.

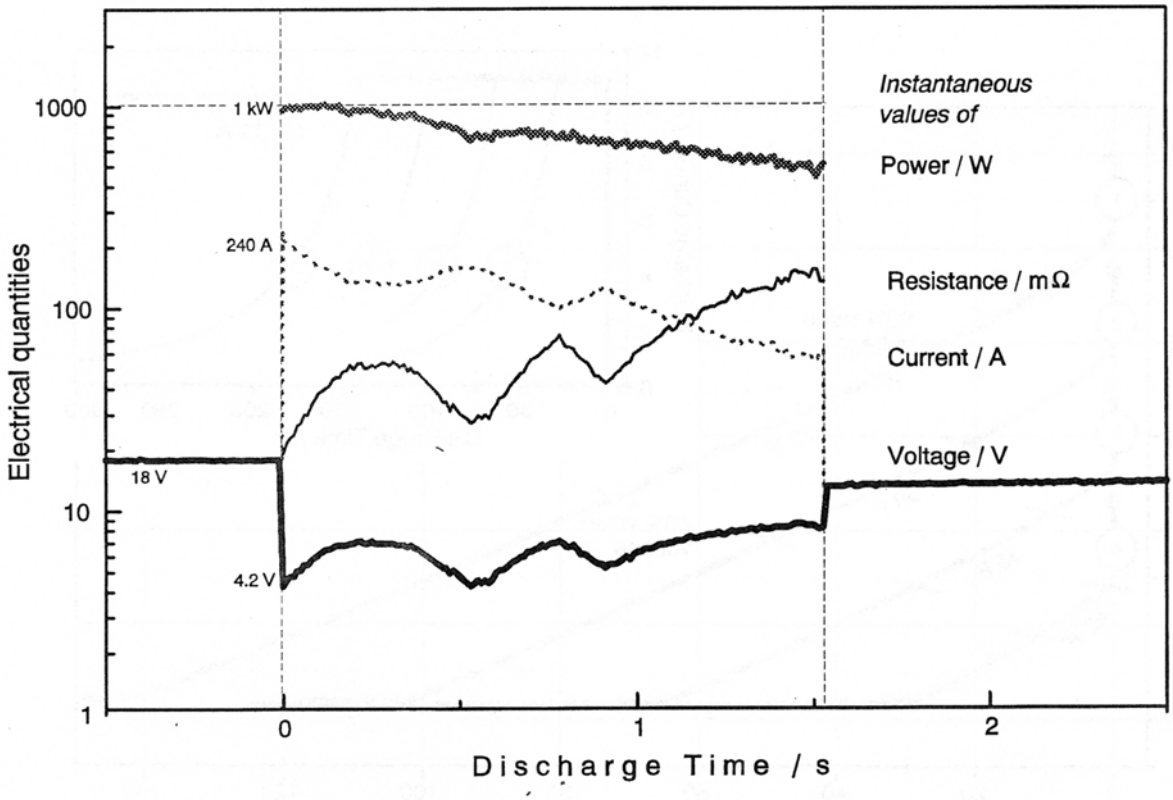

FIGURE 0.3: Transients of power demand, capacitor voltage and current, and total resistance while starting a MERCEDES C220. Ambient temeperature 12 °C, extraordinary contact resistance.

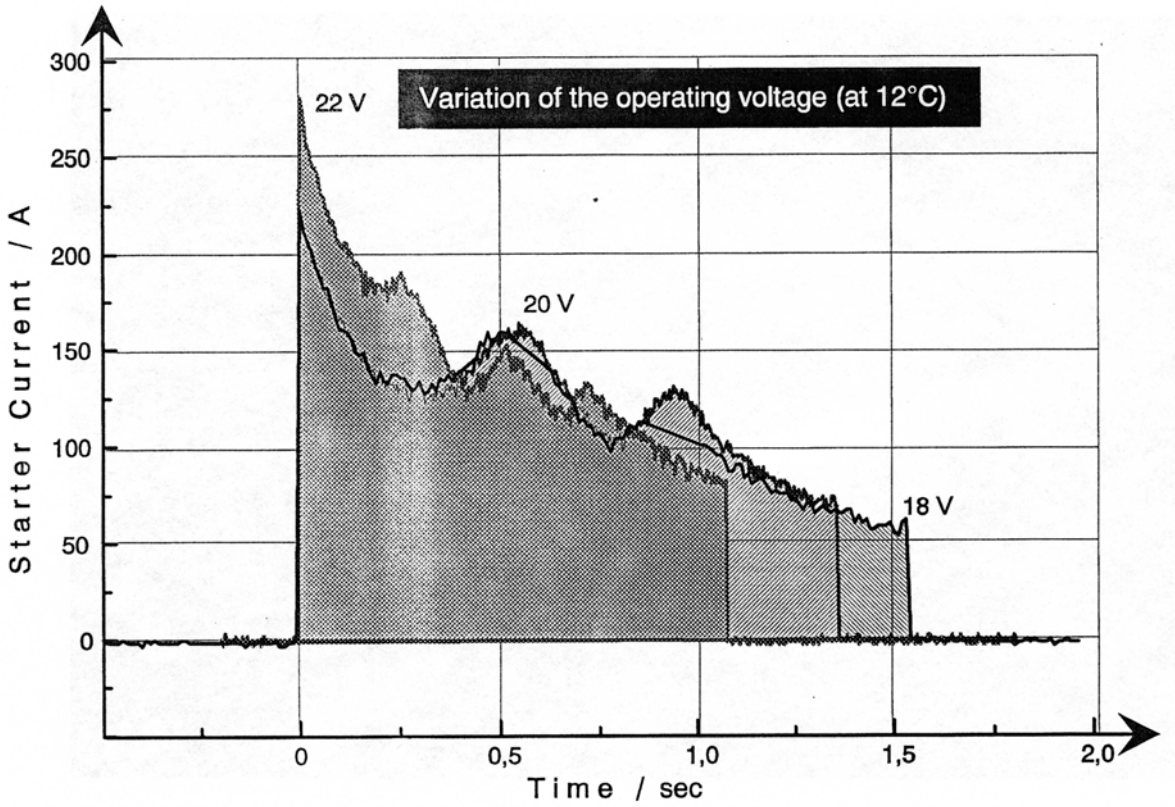

FIGURE 0.4: Variation of the operating voltage: The higher the initial voltage of the capacitor the shorter is the cranking time.

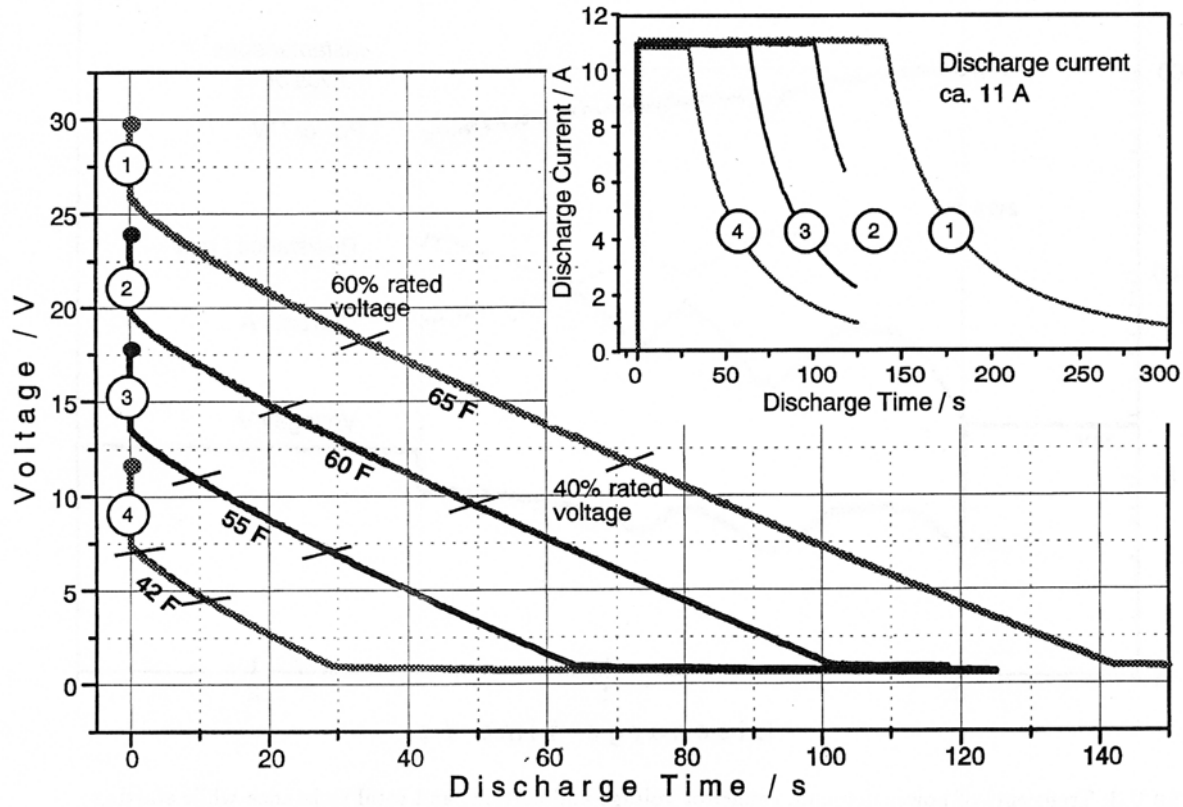

FIGURE 0.5: Determination of capacitances from discharge characteristics according to EUCAR regulations. Example: The starter capacitor after long-time testing.

TEST RESULTS

Capacitance Measurement

EUCAR Method. The rated capacitance of the 30 V capacitor was determined according to the recommendations of EUCAR, an European association supported by DAIMLER-BENZ, FIAT, Opel, PSA, Renault, Rover, Volkswagen, Volvo: „The capacitance is the reference parameter of the state of activity for supercapacitors. The changes of this parameter provides important data on energy availability and the aging of the cells" [7]. The capacitances of the cells in a pack should not differ significantly, in order to ascertain uniform behavior, which would otherwise result in a heterogeneous cell voltage distribution. The capacitance measurement is performed at three temperature levels (−20 °C, room temperature, +40 °C).

Step 1: Short circuit of each cell.

Step 2: Standard charge: At rated voltage and current limited to 50 mA/F for 1 hr at room temperature.

Step 3: Acclimatisation: The rated voltage remains applied at test temperature.

Step 4: Discharge at a current of 5 **mA/F** (single cell); end of discharge: voltage ≤10% of the rated voltage (at test temperature).

Figure 0.5 shows the characteristics of a 30 V supercapacitor, which was discharged by means of an electronic load drawing a current of

$$0.005\ \text{A} \cdot 30\ \text{cells} \cdot 70\ \text{F} \approx 10.5\ \text{A}.$$

According to EUCAR, capacitance is calculated by using the following formula:

$$Q = I \cdot (t_2 - t_1) \qquad (0\text{-}5)$$

$$C = \frac{Q}{U_1 - U_2} \qquad (0\text{-}6)$$

U_1, U_2 are the initial and final voltage, corresponding to 60% and 40% of the rated voltage.

t_1, t_2 are the times when U_1, U_2 are reached.

Q means the electric charge.

Method 2. We contrasted the simple EUCAR test procedure with a method derived from the following definition of capacitance:

$$C = \frac{\mathrm{d}Q}{\mathrm{d}U} = \frac{I\,\mathrm{d}t}{\mathrm{d}U} = \frac{I}{\dot{U}}. \qquad (0\text{-}7)$$

$\dot{U}$ is the slope of the total linear part of the voltage-time curve.
The following table illustrates that both methods lead to approximately the same results.

Table 0.1 Capacitance of a 30 V supercapacitor at different initial voltages U_1 using the EUCAR procedure and the "Cv method" according to the equation $C = I/\dot{U}$ (at room temperature).

	EUCAR method				"Cv method"		
U_1 (V)	Q (As)	Δt (s)	ΔU (V)	C (F)	$\bar{I}$ (A)	$\dot{U}$ (V/s)	C (F)
12	101	9.3	2.4	42	10.8	0.253	43
18	186	17	3.4	55	10.9	0.200	54
24	286	26	4.7	60	11.0	0.153	72
30	387	35	5.9	**65**	11.0	0.142	**77**

Charge Characteristics

Figure 0.6 shows the charge behavior of the 30 V capacitor at a constant current of 10 A. At higher charging currents the slope of the $U(t)$ curve is steeper and the rated voltage is reached earlier.

Table 0.2 Specific energy data according to the charge characteristics of the 30 V/65 F capacitor.

Voltage (V)	Active and total energy density			
	Wh/ℓ	Wh/kg	Wh/ℓ	Wh/kg
	without end plates		capacitor	
12	1.0	0.3	0.32	0.2
18	2.5	0.8	0.83	0.5
24	3.5	1.1	1.2	0.7
30	**5.0**	1.6	1.7	1.0

The energy was measured by integrating current and voltage while charging the capacitor. Specific energies up to 5 Wh/kg were achieved (see table).
Leakage current appeared to be dependend on voltage. Below 75% of the rated voltage, leakage currents do not play an important role (see Figure 0.6).

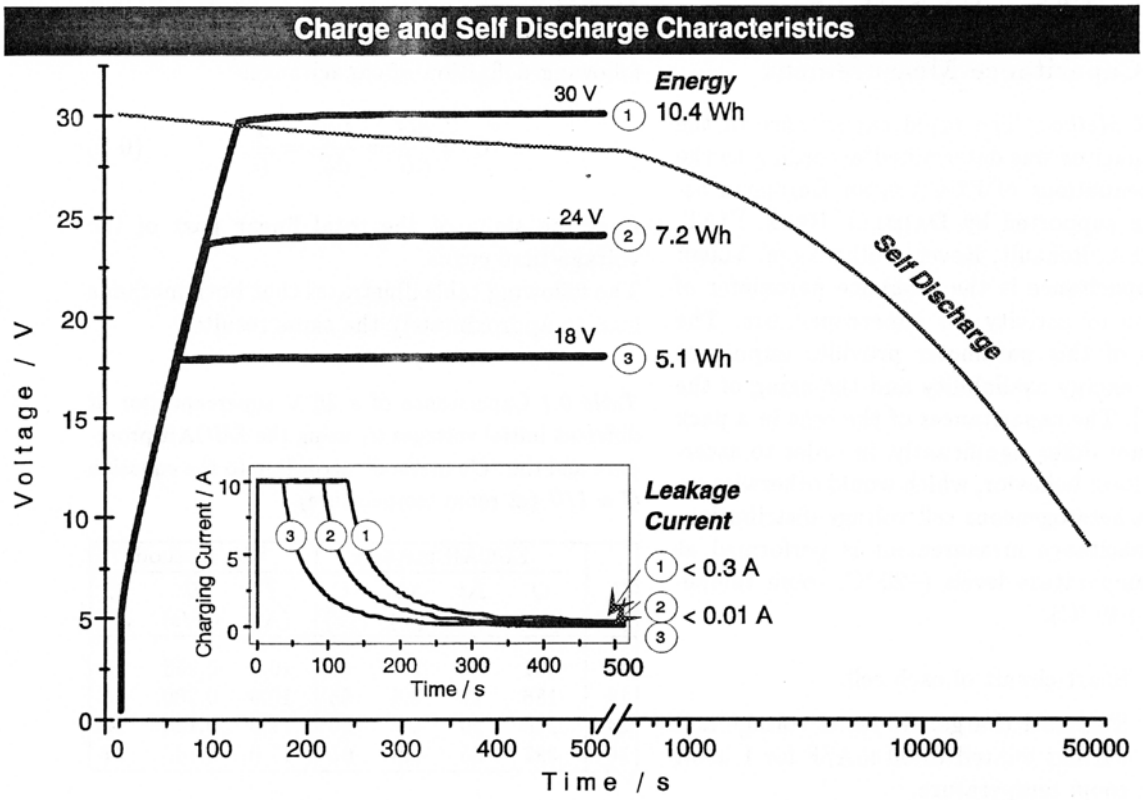

FIGURE 0.6: Charge and self-discharge behavior of the 30 V/65 F capacitor.

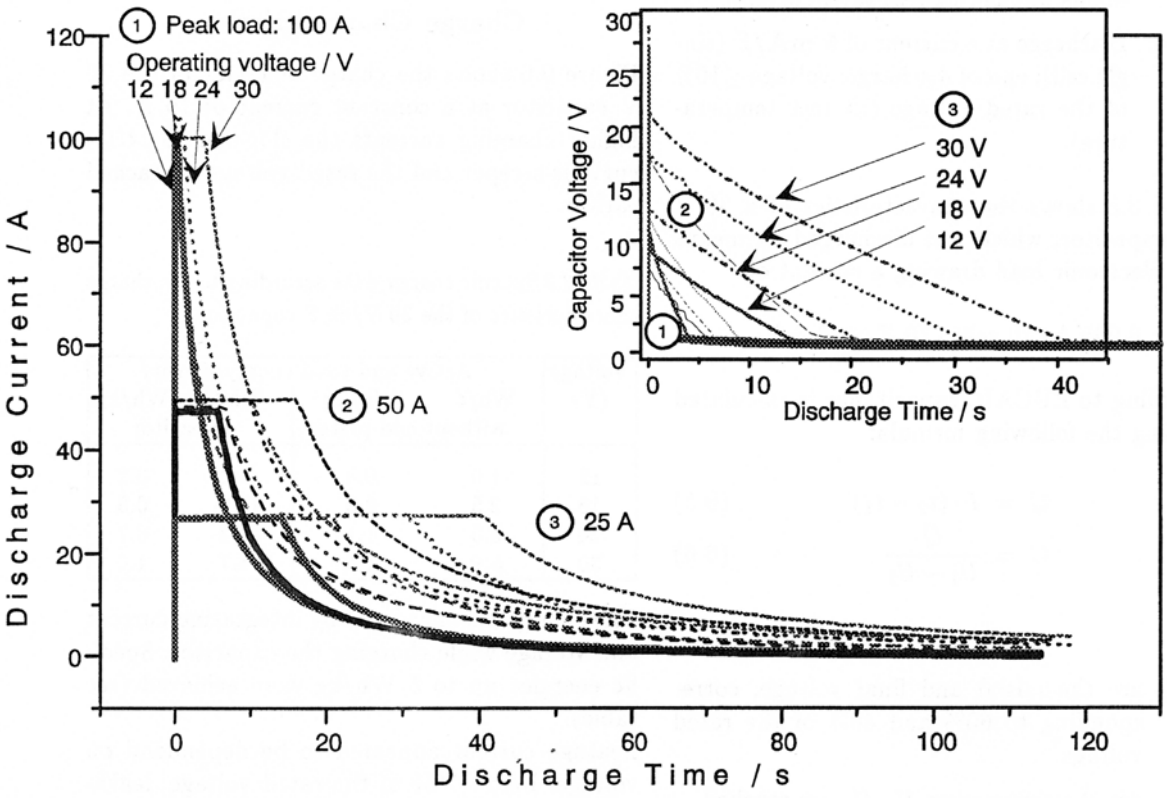

FIGURE 0.7: Discharge characteristics of a 30 V/65 F supercapacitor at different load currents.

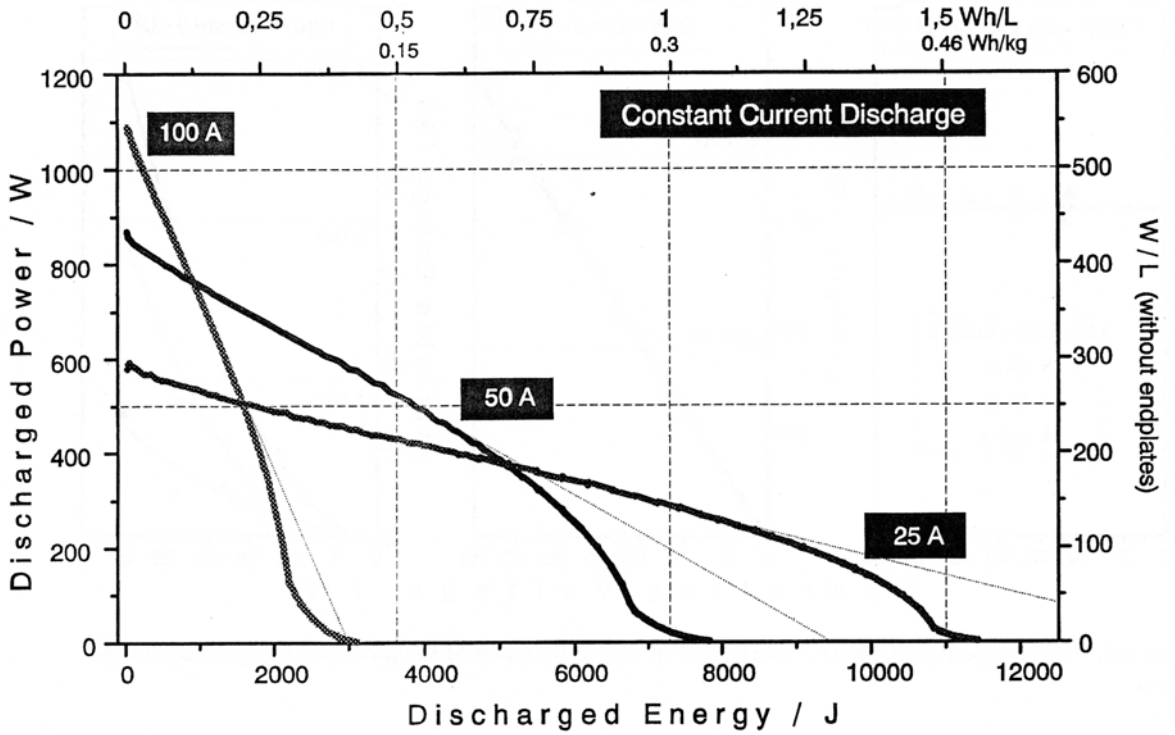

FIGURE 0.8: Specific power and energy at different discharge currents.

Discharge Characteristics

Figure 0.7 shows the discharge characteristics of a 30 V supercapacitor at different load currents and operating voltages. Currents up to 100 A were drawn for time spans ranging from seconds to minutes. The capacitor voltage decreases almost linearly (see small picture).
The discharged energies and powers are shown in Figure 0.8. At 100 A the power density of the 30 V/65 F supercapacitor equals 550 W/ℓ. Peak power densities lie in the kilowatt range (see below).

Voltage Dependence

For numerical modeling purposes of electrochemical capacitors, the capacitance, charge and energy were studied as functions of voltage. The investigation was based on the discharge characteristics shown in Figure 0.7.
At constant discharge current (25, 50 and 100 A) the electric **charge** is directly proportional to the voltage,

$$\boxed{Q(U) \approx 62.2 \cdot U}, \qquad (0\text{-}8)$$

which is consistent with the fact that the electric charge should be the product of the rated capacitance and voltage ($Q = CU$).
The **capacitance** (in Farads) seems to be an approximately linear function of the rated voltage (in Volts):

$$\boxed{C = 0.14 \cdot U + 60}. \qquad (0\text{-}9)$$

This is the mean least squares fit curve for all the measurements at 25, 50 and 100 A current flow.
Due to the electrochemical processes occuring at the electrode/electrolyte interface, supercapacitors do not share the constant capacitance over a wide voltage range, which is well known from conventional capacitors.
A more detailed analysis reveals that the linear function behavior of $C(U)$ is a only a rough approximation. A more complex dependence of capacitance on voltage can be understood by looking at the cyclic voltammogram of a supercapacitor single cell [6]: the most effective and reversible redox reactions occur when reaching 50% of the decomposition voltage of the electrolyte. This roughly corresponds to 50% rated voltage of the capacitor.

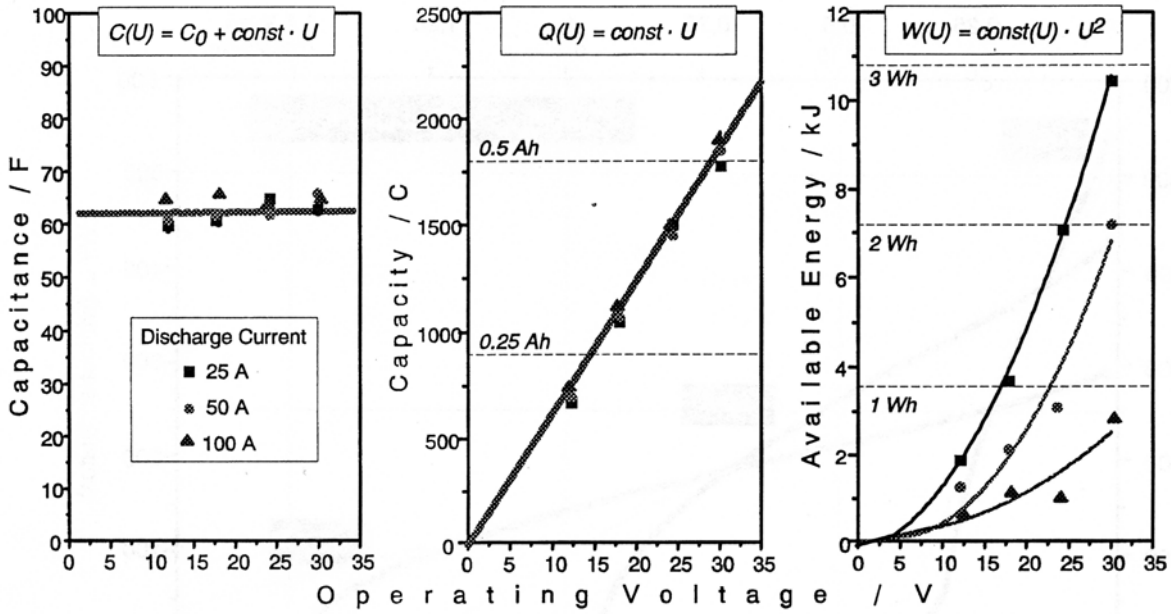

FIGURE 0.9: Usable capacitance, electric charge and energy as functions of the initial charging voltage of the capacitor.

The usable **energy** shows the expected squared dependence on voltage:

$$\boxed{W(U) \approx 30 \cdot U^2}, \qquad (0\text{-}10)$$

where the factor 30 increases with increasing current. It represents the term $\frac{1}{2}C$ of an effective capacitance C.

REFERENCES

[1] P. Kurzweil, G. Dietrich, *Double-layer capacitors for energy storage devices in space applications, Proc. 2nd Int. Seminar on Double Layer Capacitors and Similar Energy Storage Devices,* Deerfield Beach, Florida (1992).

[2] P. Kurzweil, G. Dietrich, *Supercapacitors with irresistible advantages. Link between conventional capacitors and batteries, Dornier Post,* Nr. 4 (1994) 32–33.

[3] P. Kurzweil, *Doppelschichtkondensatoren — eine Herausforderung an die Elektrochemie der Edelmetalloxide,* 2. Ulmer Elektrochemische Tage, 20.–21.06.1994, Universitätsverlag Ulm (1996).

[4] S. Trasatti, P. Kurzweil, *Electrochemical supercapacitors as versatile energy stores, Potential use for platinum metals, Platin. Metal. Rev.* **38** (1994) 46–56.

[5] P. Kurzweil, O. Schmid, *Low temperature proton conducting metal oxide supercapacitor, Meeting Abstracts,* The Electrochemical Society Fall Meeting, San Antonio, Texas, October 6–11 (1996) 825.

[6] P. Kurzweil, O. Schmid, *High performance metal oxide supercapacitors, Proc. 6th Int. Seminar on Double Layer Capacitors and Similar Energy Storage Devices,* Deerfield Beach, Florida, December 9–11 (1996).

[7] EUCAR traction Battery Working Group, *Specification of test procedures for supercapacitors in electric vehicle application,* Draft, September 1996.

Proceedings: The 7th International Seminar on Double Layer Capacitors,
Deerfield Beach, FL, U.S.A., December 8–10, 1997.

METAL OXIDE SUPERCAPACITOR FOR AUTOMOTIVE APPLICATIONS

Part II: Advanced Technology

P. KURZWEIL, O. SCHMID, A. LÖFFLER, A. KOCH
Dornier GmbH, Daimler-Benz Research Dept. F1M/BE, 88039 Friedrichshafen, Germany

Based on the results obtained by starting a car, an improved capacitor was designed and built. The capacitor's specifications are shown in Table 1:

Table 0.1 Improved supercapacitor.

	Total stack	Single cell
Voltage	15 V	1.0 V
Capacitance	100 F	1.74 F/cm^2
Resistance	2 mΩ	0.12 Ω cm^2
Cross-sect. area	1090 cm^2	863 cm^2
Thickness	4.0 cm	0.075 cm
Total volume	4.36 ℓ	—
Active volume	1.23 ℓ	0.065 ℓ
Mass	5.05 kg	0.158 kg
Endplates	2.68 kg	—
Density	1.2 g/cm^3	2.4 g/cm^3

Mass was drastically reduced by constructive efforts. The heavy endplates were replaced by light metal plates with a milled surface, which are to guarantee an improved heat mangament by thermal convection.

The individual cells were sealed with special fluorosilicon elastomers. Figure 0.2 shows a cost-effective coating technique which includes the use of a robot. The sealing material is directly applied onto the bipolar plates. Compared to conventional flat seals less space is required.

TEST RESULTS

Short-Circuit

In technical literature, the short-circuit current and power are standard reference parameters used to compare supercapacitors. We discharged the 15 V supercapacitor using a 0.1 mΩ shunt.

Table 0.2 Short-circuit experiment: Transients of current and power of a 15 V/100 F supercapacitor.

t (ms)	$I(t)$ (A)	Power kW	Power W/kg packaged	R_i mΩ
0.4	2070	26	5140	2.5
1.4	2030	21	4150	3.0
2.4	2470	11	2180	3.7
5	2360	8.5	1680	4.0
10	2260	8.1	1600	4.3
50	1910	5.9	1170	5.4
100	1680	4.5	890	6.5

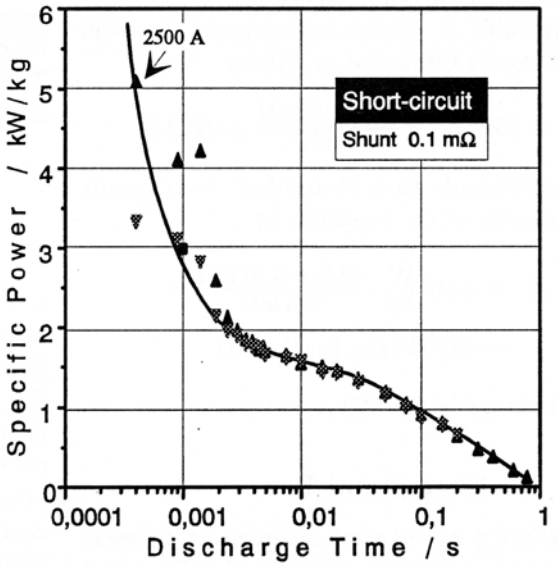

FIGURE 0.1: Short-circuit characteristic of a 15 V/100 F supercapacitor. The peak power in the micro second range exceeds 6 kW/kg.

The current and voltage of the capacitor were recorded using an oscilloscope. Several experiments were carried out to be sure that the results

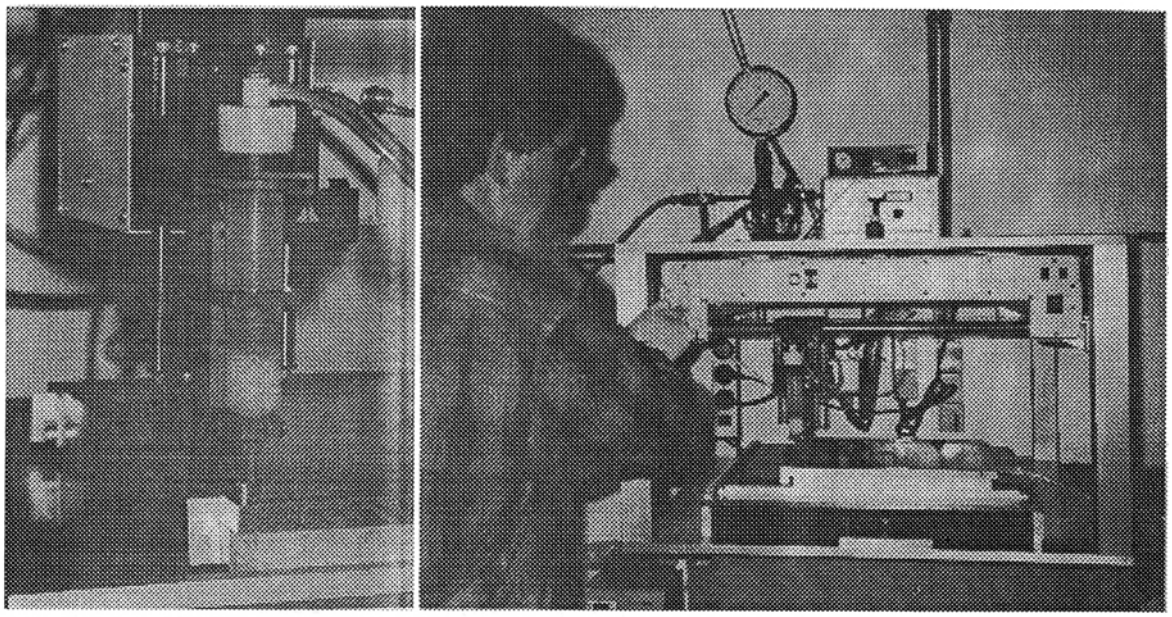

FIGURE 0.2: Manufacture of elastomer seals between bipolar plates and electrolyte.

in Table 2 and Figure 1 are correct and reproducible. The overall resistance of the shunt, switch, cables and contacts equaled 0.8 mΩ, and was subtracted from the measured resistance to yield the inner resistance R_i of the capacitor shown in Table 1.

For the hypothetical case that the capacitor is completely discharged in an electric circuit without any cable or contact resistances, the peak current can be estimated as follows:

$$I_p = 2070\,\mathrm{A} \cdot \frac{(2.5+0.8)\,\mathrm{m\Omega}}{2.5\,\mathrm{m\Omega}} = 2732\,\mathrm{A}.$$

This corresponds to a theoretical short-circuit power density of the capacitor of

$$P_p = 5140\,\frac{\mathrm{W}}{\mathrm{kg}} \cdot \frac{(2.5+0.8)\,\mathrm{m\Omega}}{2.5\,\mathrm{m\Omega}} = \\ = 6785\,\mathrm{W/kg\ (packaged)}$$

for a discharge in the 500 μs range.

Energy and Power

The discharge curves were recorded at different currents and at constant power loads. Figure 0.3 shows the RAGONE plot of the 15 V/100 F metal oxide supercapacitor. The short-circuit results are included. The power and energy densities of packaged and unpacked capacitors differ by a factor of two, which is due to the weight of the endplates.

Frequency Response

Figure 0.4 shows the frequency response of the supercapacitor. The capacitive properties of the supercapacitor are definitely guaranteed below 1000 Hz, which is a distinct advantage compared to some capacitors described in technical literature. The decline of capacitance towards high frequencies is less severe than with capacitors based on carbon materials.

The capacitance was calculated based on the admittance for every frequency:

$$\boxed{\begin{aligned} C(\omega) &= \frac{\mathrm{Im}\,\underline{Y}}{\omega} = \frac{-\mathrm{Im}\,\underline{Z}}{\omega\,|\underline{Z}|^2} \\ |\underline{Z}| &= \sqrt{(\mathrm{Re}\,\underline{Z})^2 + (\mathrm{Im}\,\underline{Z})^2} \end{aligned}}$$

$\omega = 2\pi f$ is the circular frequency. Re $\underline{Z}$ and Im $\underline{Z}$ are ohmic resistance and reactance respecticely. The capacitance reaches its maximum below 1 Hz. This is the case when there is time enough for slow electrode reactions to occur in the pores of the metal oxide. At high frequencies it is primarily the "outer" electrode surface which is charged and discharged. Accordingly, there is a strong decline of capacitance, which is related to the concentration wave penetrating into the pores. Above 5000 Hz inductive behavior plays an increasingly important role.

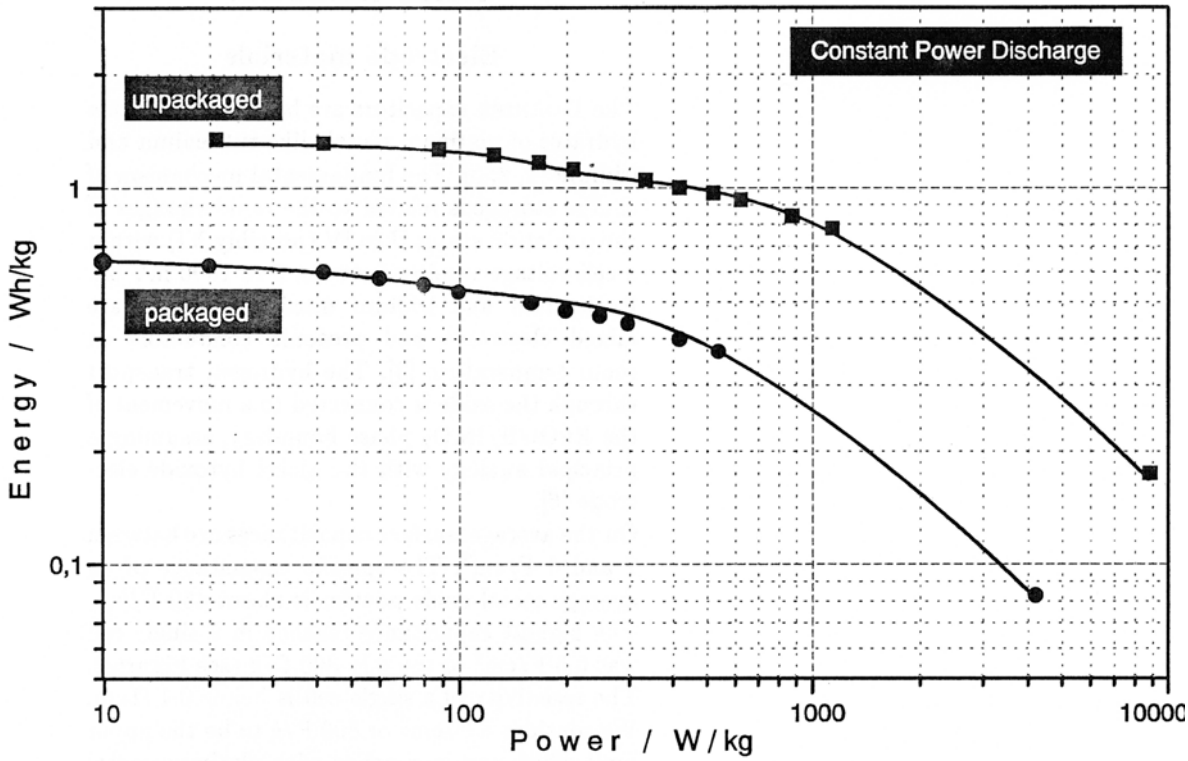

FIGURE 0.3: Usable power and energy of a 15 V/100 F supercapacitor at constant power discharge. Initial voltage 15 V (= 1 V per cell). Total weight 5.05 kg including casing.

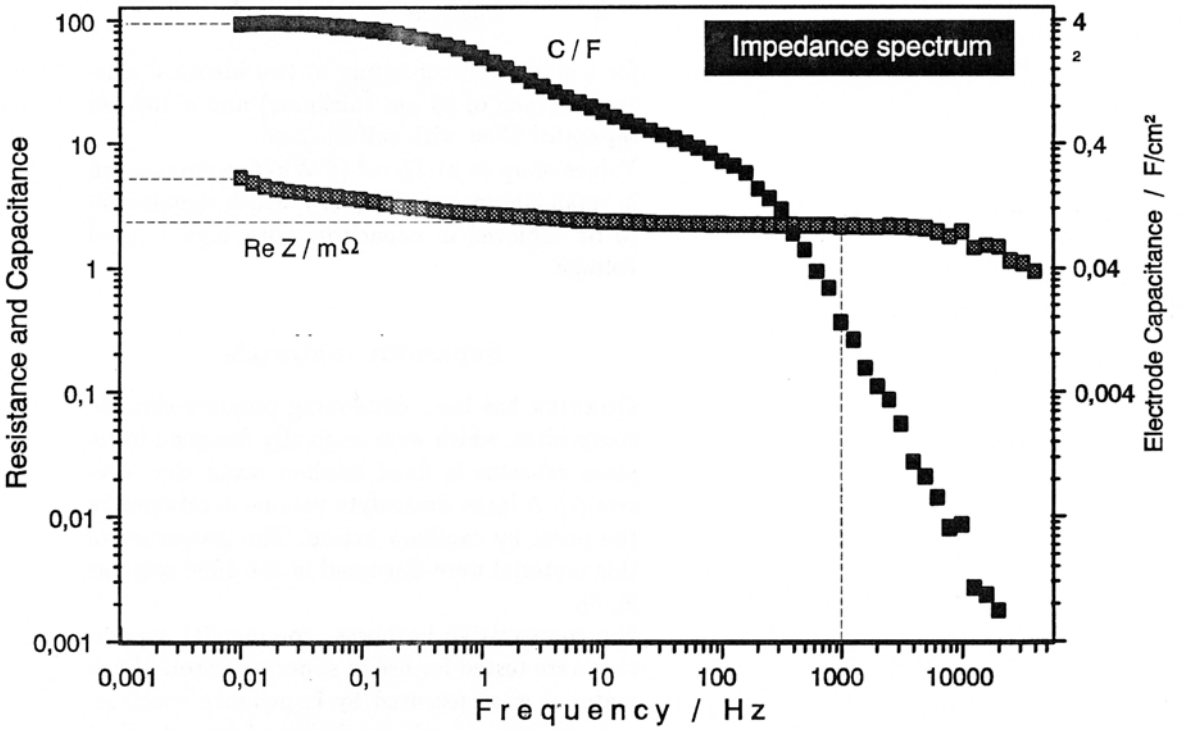

FIGURE 0.4: Frequency response of ohmic resistance and capacitance of a 15 V capacitor.

CELL DESIGN

Electrode materials

The DORNIER capacitors are based on the oxide hydrates of platinum metals like ruthenium and iridium [1, 2, 3]. The fundamental mechanism of charge storage is related to the rapid changes of the oxidation states II to IV (possibly VI) within a cell voltage window between 0 to 1000 mV [4]. Ruthenium and iridium dioxide hydrates are mixed electronic and protonic conductors at room temperature [5]. The hydrogen transport through the oxide is connected to a movement of the $RuOOH/RuO_2$ phase boundary, assuming a principal analogy with the nickel hyroxide electrode [6].

On the average, surface capacitances are between 2 and 4 F/cm^2. The specific capacitance of an average metal oxide powder is about 450 F/g. The highest capacitance reached in a single cell was 6.5 F/cm^2 or roughly 800 F/g (see Figures). The resistivity of a single cell is below 0.1 Ω cm. We consider 8 F/cm^2 or 800 F/g to be the upper limit which can be reached with platinum metal oxides on three-dimensional electrode supports. This corresponds to an energy density of

$$\frac{1}{2} \cdot \frac{\frac{1}{2} \cdot 8\,\mathrm{F/cm^2} \cdot (1\,\mathrm{V})^2}{0.028\,\mathrm{cm}} = 71 \frac{\mathrm{J}}{\mathrm{cm}^3} = 20\,\frac{\mathrm{Wh}}{\ell}$$

for a single cell consisting of two identical electrodes (each of 90 μm thickness) and a 100 μm separator filled with sulfuric acid.

Values of up to 21 J/cm^3 (6 Wh/ℓ) were realized in small laboratory cells (1 V), which remains yet to be achieved in capacitors with higher rated voltage.

Separator materials

DORNIER has been developing polymer-ceramic composites, which were originally designed to replace asbestos in fixed alkaline water electrolysers [7]. A large electrolyte volume is retained in the pores by capillary action. The properties of this material were discussed in the 1996 seminar [6, 8].

For comparative purposes, commercial separators were tested for use in supercapacitors. Each material was measured by impedance spectroscopy in a single cell consisting of two identical metal oxide electrodes of 0.3 mm thickness. The results are shown in Table 0.3.

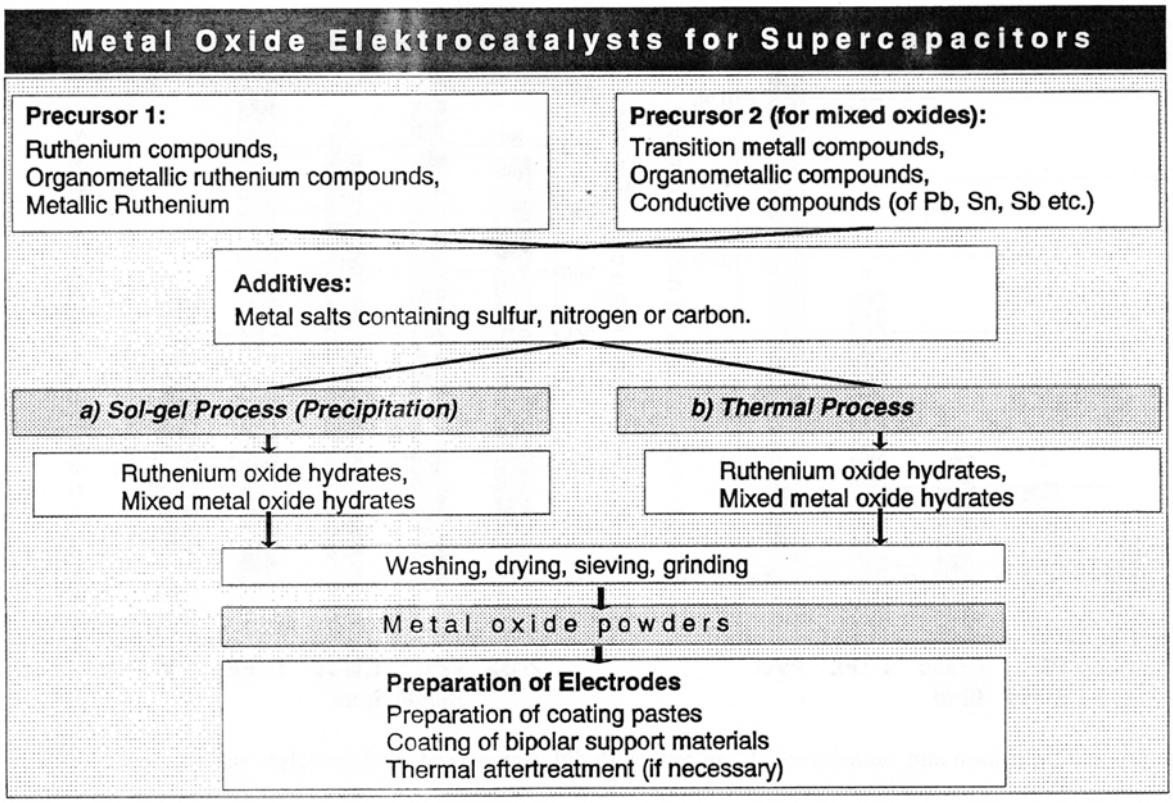

FIGURE 0.5: Synthesis of mixed metal oxide electrocatalysts for supercapacitors (patent granted).

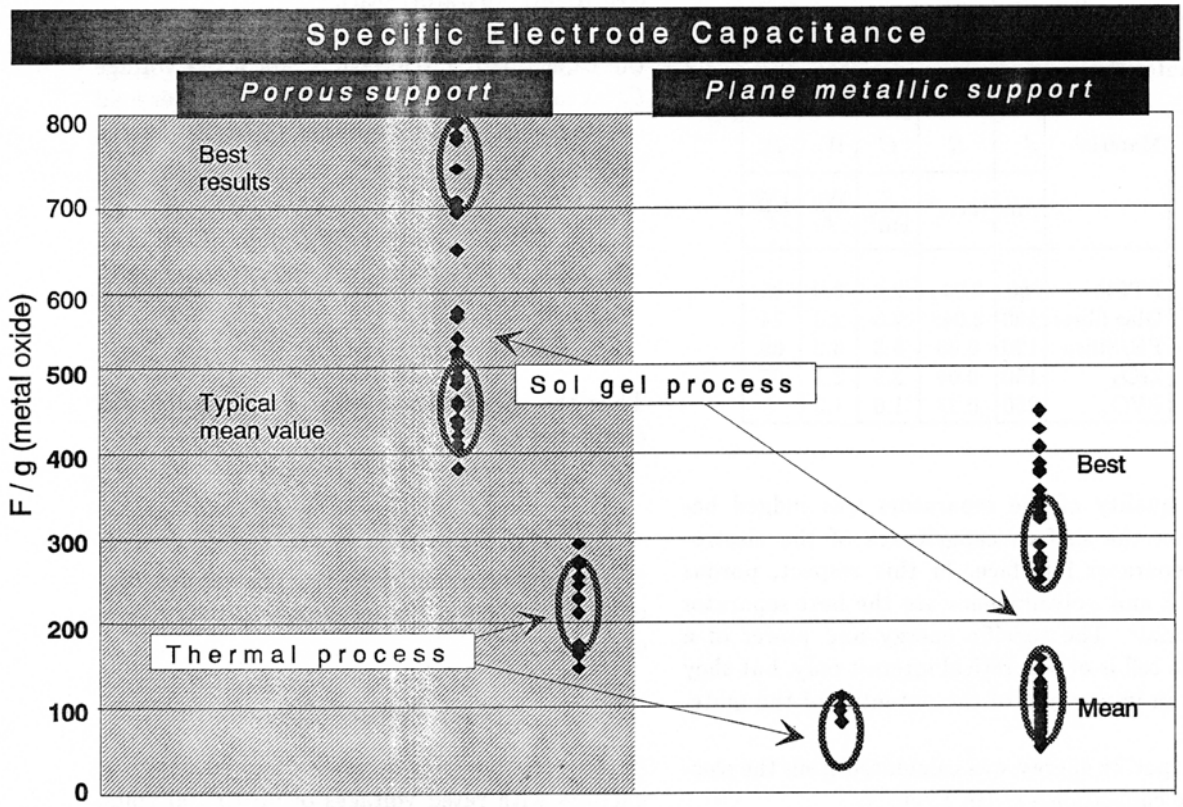

FIGURE 0.6: Mass-specific capacitance of the metal oxide depending on the preparation method. Impedance measurements of single cells (at 0.1 Hz).

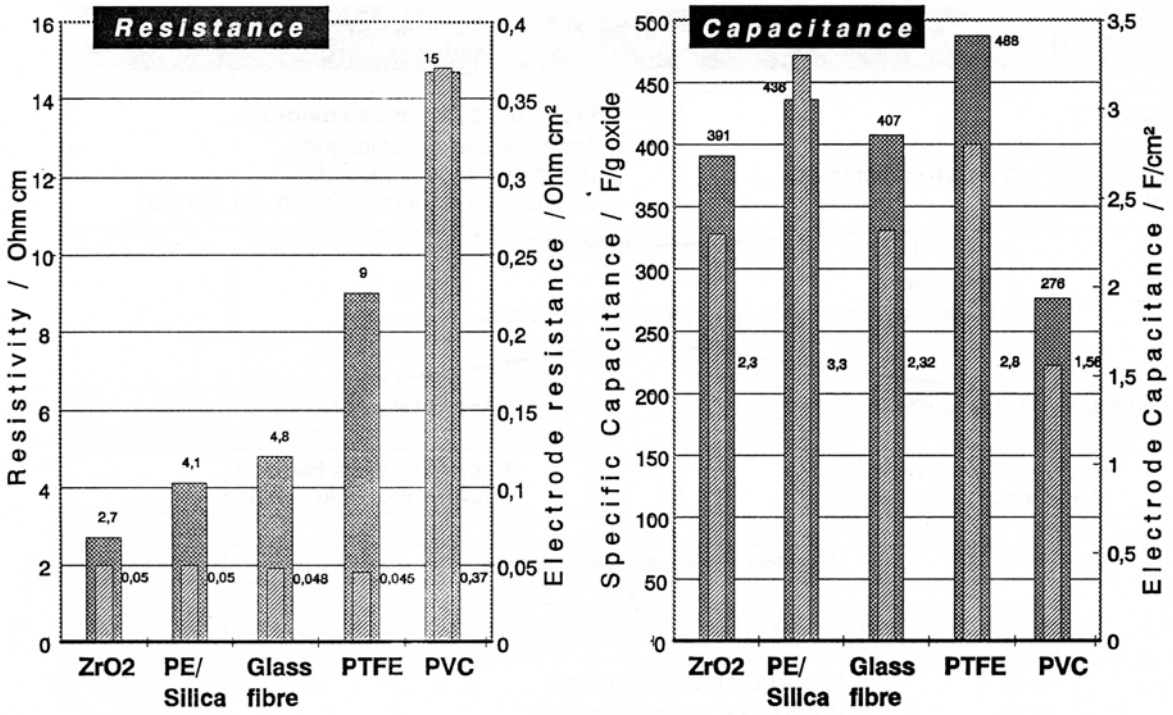

FIGURE 0.7: Resistance and capacitance of half cells with different separators. Electrolyte sulfuric acid.

Table 0.3: Evaluation of different separators for use in supercapacitors: R surface resistance, C electrode capacitance, W_v energy density, P_v power density, d separator thickness.

Material	d	R	C	W_v	P_v
	μm	$\Omega\,\mathrm{cm}^2$	$\frac{\mathrm{F}}{\mathrm{cm}^2}$	$\frac{\mathrm{Wh}}{\ell}$	$\frac{\mathrm{kW}}{\ell}$
PTFE	50	0.045	2.8	3.0	85
Glas fibres	100	0.048	2.3	2.3	74
PE/Silica	120	0.05	3.3	3.2	69
ZrO_2	150	0.05	2.3	2.1	67
PVC	250	0.37	1.6	1.3	8

The quality of the separators was judged based on the surface capacitance of the electrode/separator interface. In this respect, porous PTFE and polyalkylenes are the best separator materials. The specific energy and power of a single cell is of theoretical interest only, but they give an impression of the potential of the materials.

The specific energy was calculated from the electrode capacitance C (in $\mathrm{F/cm}^2$):

$$W_v = \frac{1}{d_{cell}} \left[\frac{1}{2} \left(\frac{1}{2} C \right) (1\ \mathrm{V})^2 \right] ,$$

where d_{cell} is the total thickness of the cell (two electrodes, separator, seal).

The peak power was calculated for the case that the capacitor is discharged at its rated voltage U_n at maximum power, i.e. when the outer load resistance R_v equals the inner resistance of the capacitor R_i:

$$\begin{aligned} P &= I^2 R_v = \left(\frac{U_n^2}{R_v + R_i} \right)^2 R_v \\ P_{max} &= \frac{\mathrm{d}P}{\mathrm{d}R_v} \stackrel{!}{=} 0 \quad \Rightarrow \quad R_v = R_i . \\ P_{max} &= \frac{1}{4} \frac{U_n^2}{R_i} \end{aligned}$$

Thus the specific peak power in Table 0.3 was calculated as:

$$\boxed{P_v = \frac{1}{d_{cell}} \left[\frac{1}{4} \frac{U_n^2}{R_i} \right]} .$$

The results represent short-term power densities only. Nevertheless, the technological potential is obvious.

Near Future Goals

DORNIER is planning to realize bipolar supercapacitors with rated voltages of up to 100 volts, energy densities ranging from 3 to 7 Wh/kg (packaged), and power densities between 10 and

40 kW/kg. Future commercial applications will require a further mass and metal oxide reduction.

REFERENCES

[1] P. Kurzweil, O. Schmid, B. Schmid, DE 43 13 474, EP 0 622 815, US 5 550 706.

[2] S. Trasatti, Electrodes of conductive metallic oxides, Part A, pp. 332ff, Elsevier, Amsterdam (1980).

[3] K. Doblhofer, M. Metikos, Z. Ogumi, H. Gerischer, *Electrochemical oxidation and reduction of the RuO_2/Ti electrode surface*, *Ber. Bunsenges. Phys. Chem.* **82**, 1946–1050 (1978).

[4] S. Trasatti, P. Kurzweil, *Electrochemical supercapacitors as versatile energy stores, Potential use for platinum metals*, *Platin. Metal. Rev.* **38** (1994) 46–56.

[5] P. Kurzweil, O. Schmid, *Low temperature proton conducting metal oxide supercapacitor*, *Meeting Abstracts*, The Electrochemical Society Fall Meeting, San Antonio, Texas, October 6–11 (1996) 825.

[6] P. Kurzweil, O. Schmid, *High performance metal oxide supercapacitors*, *Proc. 6th Int. Seminar on Double Layer Capacitors and Similar Energy Storage Devices*, Deerfield Beach, Florida, December 9–11 (1996).

[7] O. Schmid, U. Benz, W. Tillmetz, *Electrolysis in space*, *Proc. Europ. Space Power Conf.*, Graz, 23–27 August 1993, 663–669.

[8] O. Schmid, G. Toth, W. D. Vogel, R. Ostertag, *Asbestfreie Diaphragmen für alkalische Zellen*, *GDCh-Monography* "Elektrochemie und Werkstoffe", VCH Weinheim 1995.

Proceedings: The 7th International Seminar on Double Layer Capacitors,
Deerfield Beach, FL, U.S.A., December 8–10, 1997.

METAL OXIDE SUPERCAPACITOR FOR AUTOMOTIVE APPLICATIONS

Part III: Heat Management

P. KURZWEIL, M. SEIFERT, R. SONNENSCHEIN, O. SCHMID

Dornier GmbH, Daimler-Benz Research Dept. F1M/BE, 88039 Friedrichshafen, Germany

The temperature distribution in a supercapacitor was modeled as a function of the discharge parameters. The maximum temperature in the center of the stack was calculated for the case that a car is cranked continously in urban stop-and-go traffic.

BASIC TREATMENT

The starting point of the calculation is FOURIER's equation of thermal conductivity:

$$\boxed{\varrho\, c_p \frac{\partial T}{\partial t} = \operatorname{div}(\lambda \operatorname{grad} T) + \frac{\dot{Q}}{V}} \qquad (0\text{-}1)$$

T Thermodynamic temperature (K),
λ thermal conductivity of the capacitor ($\mathrm{W\,K^{-1}m^{-1}}$),
ϱ mean density of the capacitor ($\mathrm{kg\,m^{-3}}$),
c_p mean specific heat capacity ($\mathrm{J\,kg^{-1}K^{-1}}$),
$\dot{Q}$ mean thermal output, heat flow rate (W),
V volume of the capacitor ($\mathrm{m^3}$).
$\dot{Q}/V$ average volume heat flux ($\mathrm{W/m^3}$).

This differential equation was solved using the boundary condition:

$$\boxed{\lambda \left.\frac{\partial T}{\partial t}\right|_{endplate} = \alpha\,(T_{endplate} - T_{amb})} \qquad (0\text{-}2)$$

The engineering model was based on the following assumptions:

- The capacitor is solely cooled by **natural convection** without any need of an extra fan. The endplates are vertical to the ground.
- The most effective cooling areas are the endplates of the capacitor (see Figure 2 in Part I). The heat flow through the side walls, which is comparatively small, is reflected in a three-dimensional model.
- The components of the supercapacitor were taken to be homogenous, so that a mean temperature profile may be calculated. The anisotropy of heat conductivity was considered by a tensor:

$$\lambda = \begin{pmatrix} \lambda_x & 0 & 0 \\ 0 & \lambda_y & 0 \\ 0 & 0 & \lambda_z \end{pmatrix}$$

- The heat transport within the capacitor is relatively slow, so that heat production can be averaged over time.

Thermal Output

The thermal output $\dot{Q}$ was calculated using the ohmic losses occuring at the inner resistances of the capacitor. The capacitor was described by an equivalent series network, comprising a parallel combination of a resistance R_p and a capacitance C, and a resistance R_s in series.

$$\boxed{\dot{Q} = \frac{1}{\Delta t}\int_0^{\Delta t}\left[R_s\, I^2(t) + \frac{1}{R_p}\,(U(t) + R_s\, I(t))^2\right] \mathrm{d}t} \qquad (0\text{-}3)$$

Δt time for charge or discharge respecitively (s),
R_s series or "electrolyte" resistance (Ω),
R_p parallel, "polarization" or "leakage" resistance (Ω),
I electric current through the capacitor (A),
U voltage at the endplates of the capacitor (V).

The experimental transients of current and voltage, which were used to model the starter capacitor, are shown in Figure 3 in Part I.

Coefficient of heat transfer

The heat transfer between endplates and ambient air is described by means of the coefficient α. It was calculated using tabulated material parameters for heat transfer, free convection and thermal radiation.

$$\alpha(\bar{T}) = \underbrace{\frac{\varepsilon\sigma\left(\bar{T}^4 - T_{amb}^4\right)}{\bar{T} - T_{amb}}}_{\text{radiation}} + \underbrace{\frac{\mathrm{Nu}(\bar{T})\,\lambda_{air}}{L}}_{\text{convection}} \tag{0-4}$$

$\bar{T}$ Mean temperature at the surface of the endplates of the capacitor (K),

T_{amb} ambient temperature (K),

d thickness of the components of the capacitor (m),

λ_{air} thermal conductivity at mean temperature between capacitor surface and ambient air ($\mathrm{W\,K^{-1}m^{-1}}$).

ε emittance of the endplates (—),

σ STEFAN-BOLTZMANN constant: $5.6697{\cdot}10^{-8}\ \mathrm{W\,m^{-2}K^{-4}}$,

Nu NUSSELT number for convection (—).

PROCESS DESCRIPTION

The temperature distribution was calculated for a supercapacitor which is continously charged and discharged. The numerical calculation works according to the following steps:

1. Input parameters

- Read experimental data of time t, current $I(t)$ and voltage $U(t)$ from input file (see for example Figure 2 in Part I).
- Read series and parallel resistances (R_s, R_p), which are determinded by impedance spectroscopy and leakage current measurement.
- Read lengths L, widths b, thicknesses d and coefficients of heat transfer λ of all capacitor components:
  - ▷ Endplates: $\lambda_{end} = 220\ \mathrm{W\,K^{-1}m^{-1}}$,
  - ▷ Sealing: $\lambda_{seal} = 0.2\ \mathrm{W\,K^{-1}m^{-1}}$,
  - ▷ Bipolar plates: $\lambda_{bp} = 22\ \mathrm{W\,K^{-1}m^{-1}}$.
- Read ambient temperature: $T_{amb} = -50$ to $120\,^{\circ}\mathrm{C}$.
- Read emittance of endplates: $\varepsilon \approx 0.83$.
- Read operating voltage: $U_n = 30...100$ V.
- Read duty cycle (see section „Results“).

2. Preliminary calculations

- Volume of capacitor stack: $V \approx 2000\ \mathrm{cm^3}$.
- Thermal conductivities in the stack:

$$x\text{-direction: } \lambda_x = \frac{1}{d_{cell}} \sum_i d_i\,\lambda_i$$

$$y\text{-direction: } \lambda_y = \lambda_x$$

$$z\text{-direction: } \lambda_z = \left(\frac{1}{d_{cell}} \sum_i \frac{d_i}{\lambda_i}\right)^{-1}$$

The mean heat transfer coefficient of the capacitor:

$$\lambda_m = \frac{\lambda_x + \lambda_y + \lambda_z}{3} \approx 2.3\ \mathrm{W\,K^{-1}m^{-1}}.$$

For a simple approach, the anisotropy of the thermal conductivities can be considered using a geometric scaling (together with the heat transfer coefficient):

$$\begin{aligned} s_{x,y} &= \sqrt{\lambda_z/\lambda_{x,y}} \ll 1 \\ \hat{x} &= s_x\,x, \quad \hat{y} = s_y\,y, \quad \hat{z} = z, \text{and} \\ \hat{\alpha}_{x,y} &= s_{x,y}\,\alpha_{x,y}, \quad \hat{\alpha}_z = \alpha_z \end{aligned}$$

- Leakage current:
  $$I_{leak} = U_n/R_p \approx 1.5\ \mathrm{mA},$$
  and leakage volume heat flux:
  $$U\,I_{leak}/V \approx 0.02\ \mathrm{W}/\ell.$$
- Mean thermal output in the electrolyte:
  $$P_s(t) = R_s\,I(t)^2,$$
  and due to electrode reactions:
  $$P_p(t) = \frac{1}{R_p}\,(U(t) + R_s\,I(t))^2.$$
- Volume thermal output during discharge:
  $$\dot{Q}/V \approx 197\ \mathrm{W}/\ell.$$

3. Coefficient of heat transfer

The coefficient of heat transfer α for the phase boundary between a plane metal plate surface and surrounding air is calculated according to equation (0-4). PRANDL, GRASHOF, RAYLEIGH and NUSSELT number were determined using the following formula [4]:

a) Vertical plate of height L

$$Nu = \left[0.825 + \frac{0.387\,Ra^{1/6}}{\left[1 + \left(\frac{0.492}{Pr}\right)^{9/16}\right]^{8/27}}\right]^2 \tag{0-5}$$

b) Horizontal plate of thickness L

$$\boxed{Nu = \begin{cases} 0.7\,Ra^{1/4} & \text{for } Ra < 4{\cdot}10^7 \\ 0.155\,Ra^{1/3} & \text{for } Ra \geq 4{\cdot}10^7 \end{cases}} \quad \text{(0-6)}$$

where

$$Ra = Gr \cdot Pr$$

$$Gr = \frac{9.81\,\mathrm{m/s^2} \cdot L^3\,\beta_{air}\,(T - T_{amb})}{\nu_{air}^2}$$

$$Pr = 0.7$$

$$L = 30\,\mathrm{cm}$$

β_{air} and ν_{air} depend on temperature, values are taken from literature [4] at mean temperatures $T_m = \frac{1}{2}(T_s - T_\infty)$ between capacitor surface (s) and a point outside the boundary layer (∞). Depending on the ambient temperature, the coefficient of heat transfer ranges from 6 to 12. A typical value for 20 °C ambient temperature and 35 °C within the capacitor is $\alpha = 9.2\,\mathrm{W\,K^{-1}m^{-2}}$. Figure 0.8 shows α for different temperatures.
The above engineer's formula of the Nusselt number is only a rough approximation for the local heat transfer, since it does not give any information on the local boundary layer thickness. It does not contain the interactions between the endplates and the vertical side walls of the capacitor.

4. α of the capacitor

The heat transfer coefficient for the endplates and the side walls of the capacitor at a given mean temperature $\bar{T}$ (determined iteratively, see 6.) is calculated as:

$$\alpha_{end} = \frac{1}{\frac{d_{end}}{\lambda_{end}} + \frac{1}{\alpha(\bar{T})}}$$

$$\alpha_{bp} = \frac{1}{\frac{d_{bp}}{\lambda_{bp}} + \frac{1}{\alpha(\bar{T})}}$$

$$\alpha_{seal} = \frac{1}{\frac{d_{seal}}{\lambda_{seal}} + \frac{1}{\alpha(\bar{T})}}$$

$$\alpha_{stack} = \frac{1}{d_{cell}} \Big[(d_{cell} - d_{bp})\,\alpha_{seal}(\bar{T}) + d_{bp}\alpha_{bp}(\bar{T}) \Big]$$

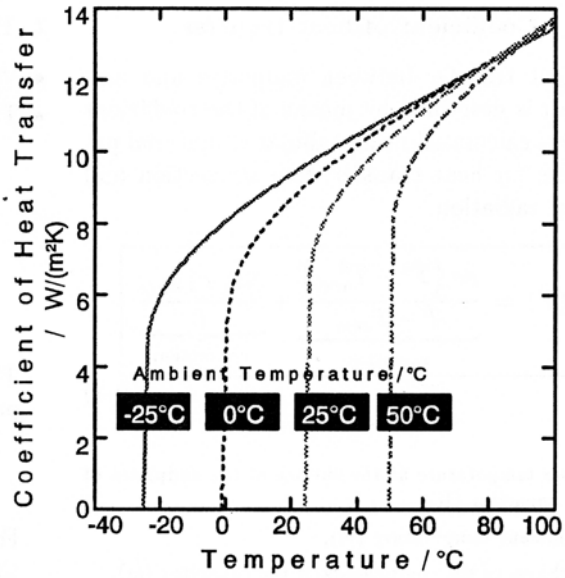

FIGURE 0.8: Heat transfer coefficient of the 30 V/65 F starter capacitor at different temperatures.

bp represents bipolar plate; *cell* denotes a single cell, comprising two electrodes, a separator and seals. An electrode consists of a bipolar plate, which is coated with porous layers and metal oxides on either side.

5. Temperature distribution (3D Model)

The stationary heat transfer equation (1) was numerically solved [1, 2, 3] to yield the three-dimensional temperature distribution in the capacitor.
In order to save computing time, one forth of the capacitor's cross sectional area was considered, since the cells are completely symmetrical. The same cooling conditions are assumed for the complete surface of the capacitor. (Natural convection does not always meet this demand.)

6. Analytical Treatment (2D)

The temperature distribution for the given geometry of the capacitor is approximately given by:

$$T(x,y,z) = \quad \text{(0-7)}$$

$$= T_{amb} + a(T)\,x^2 + b(T)\,y^2 + c(T)\,z^2 + d(T) +$$

$$+ \sum_{n=1}^{\infty} \chi_n \cos(k'_n x) \cos(k'_n y) \cosh\sqrt{2\frac{\lambda_x}{\lambda_z}}\,k'_n z$$

$$+ \sum_{n=1}^{\infty} \zeta_n \cosh \frac{k_n'' x}{\sqrt{2\lambda_x/\lambda_z}} \cosh \frac{k_n'' y}{\sqrt{2\lambda_x/\lambda_z}} \cos(k_n'' z).$$

where k_n' and k_n'' are the solutions of the following equations [5]:

$$k_n' = \frac{\alpha_{stack}}{\lambda_x} \cot\left(k_n' \frac{L}{2}\right)$$

$$k_n'' = \frac{\alpha_{end}}{\lambda_z} \cot\left(k_n'' \frac{d}{2}\right)$$

The coefficients χ_n and ζ_n are obtained by minimizing the deviations between the calculated temperature distributions and the solution fulfilling the boundary conditions. For a first approximation, the consideration of the first term ($n = 1$) is sufficient.
The coefficients of equation (0-7) read approximately:

$$d(T) = \frac{\dot{Q}/V}{\frac{4\alpha_{stack}\lambda_x}{\lambda_x b + \frac{1}{4}b^2\,\alpha_{stack}} + \frac{2\alpha_{end}\lambda_z}{\lambda_z d + \frac{1}{4}d^2\,\alpha_{end}}}$$

$$a(T) = \frac{-\alpha_{stack}}{\lambda_x b + \frac{b^2}{4}\,\alpha_{stack}}\, d(T)$$

$$b(T) = a(T)$$

$$c(T) = \frac{-\alpha_{end}}{\lambda_z d + \frac{d^2}{4}\,\alpha_{end}}\, d(T)$$

7. Mean temperature

To calculate the mean temperature $\bar{T}$ at the surface of the endplates (or side walls respectively) in contact to the ambient air, equation 0-7 is solved iteratively, starting with an intial value of $\bar{T}_1 = 400$ K.

$$\bar{T}_{k+1} = \bar{T}\Big(\alpha(\bar{T}_k)\Big). \qquad (0\text{-}8)$$

RESULTS

Maximum Temperature

One of the most important parameters is the maximum temperature that is reached in the capacitor during continous operation with intermittent or variable loads.
The discharge characteristic of the capacitor during cranking (shown in Part I) is considered to be a repeated process with a frequency that is given by the **duty cycle**:

$$\boxed{\text{Duty Cycle} = \frac{t_{dis}}{t_{ch} + t_{leak} + t_{dis}}}\,.$$

t_{ch} Time for charging (s),

t_{dis} Time for discharging or pulse duration(s),

t_{leak} Time between charging and discharging, during which leakage currents flow, when the capacitor is not used (s).

Reasonable values for the duty cycle are numbers between 0 and 1 and can be expressed by a ratio, for example 1 : 100 for a 1-second discharge and 100-second charging cycle.
The value of duty cycle is large when the capacitor is pulse-operated, i.e. when it is repeatedly charged and discharged for extended operation time. In this operating mode the capacitor may approach critical temperatures which can cause failure.
The duty cycle is small, when the period of charging is long against the period of discharging. In addition to the heat-up during discharge, leakage currents have to be considered.
Figure 0.9 shows that critical temperatures are hardly ever reached when the supercapacitor is given time enough for recharging. Only cooling by natural convection was permitted. The distribution of temperature is drastically improved when using a fan. The solid lines show the maximum temperatures in the center of the stack and the dashed lines the maximum temperatures at the surface of the endplates, which are in contact to the ambient air.
When the duty cycle turns to one, i.e. when the time for charging and discharging are the same, temperatures of up to 110 °C may be reached in the center of the capacitor after a more or less extended period of continous operation at elevated ambient temperatures. Thus, the figure gives a citerion for stable and secure operation of the capacitor: As long as the duty cycle does not exceed 1 : 8, and ambient temperature stays below 50 °C, continous operation is guaranteed for a prolonged time. This means, that the car can be started every nine seconds (assuming the capacitor can be fully charged within this intervall). *This condition is certainly fulfilled for automotive applications!*

Temperature Profiles

Other than the maximum temperature in the stack and minimum temperature at the surface of the endplates, the temperature distribution in

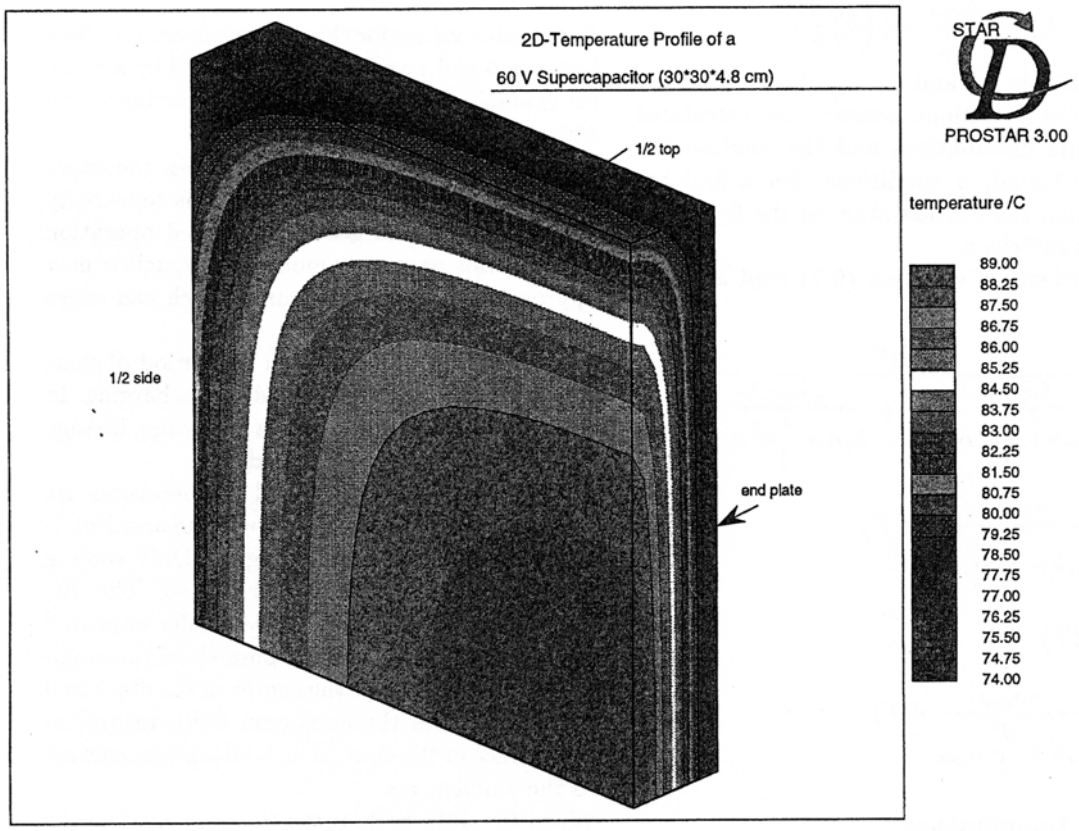

FIGURE 0.11: Temperature profile of a future **60 V supercapacitor** (30 × 30 × 4.8 cm). Stationary solution after 5–6 hrs using a finite volume method. Thermal output 40 W/ℓ. Cooling by natural convection only in ambient air of 20 °C. One forth of the actual cross sectional area is shown.

a single cell is most definitely an important parameter.

Figure 0.11 shows the stationary temperature profile of a future 60 V supercapacitor, which is operated at a thermal output of 40 W/ℓ. The capacitor is solely cooled by natural convection in ambient air of 20 °C. The maximum temperature in the center of the stack reaches 89 °C.

Maximum temperatures are found in the center of the cells, from where they drop off when moving towards the side walls. Under normal operation there is no strong temperature difference between the center of the stack and the side walls. At continuous pulse-operation (duty cycle near 1) the temperature gradient across each single cell is more pronounced.

Figure 0.12 shows the temperature profile of the same capacitor, when it is placed onto an insulated bottom plate.

The 30 V supercapacitor described in Part I, was considered for continously starting a car: between the endplates and the center of the capacitor, there is a temperature difference of between 1 and 5 °C, depending on the ambient temperature. This means that the heat transfer within the stack is relatively good. The heat transmisson from the endplates to the ambient air is the crucial point of the heat transfer process.

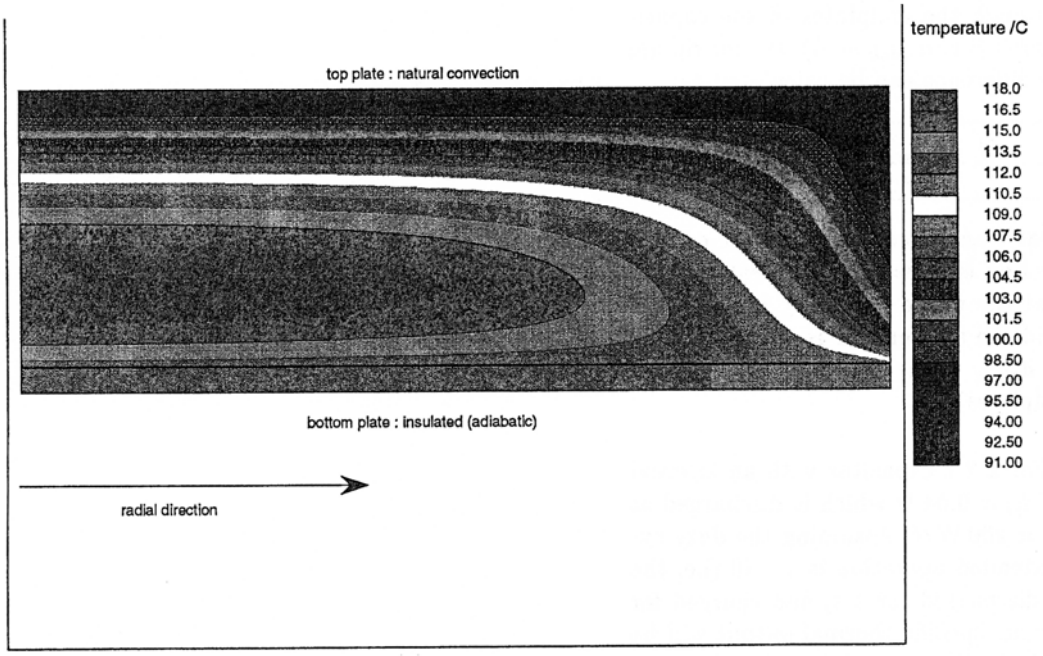

FIGURE 0.12: Temperature profile of a 60 V supercapacitor lying on an insulated bottom plate. Stationary solution after 5–6 hrs (finite volume method). Thermal output 40 W/ℓ. Cooling by natural convection only in ambient air of 20 °C.

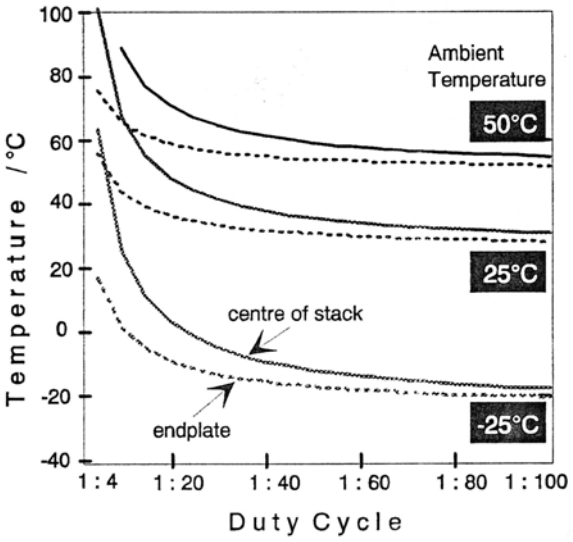

FIGURE 0.9: Maximum temperature in the center of the 30 V/65 F starter capacitor at different ambient temperatures and duty cycles.

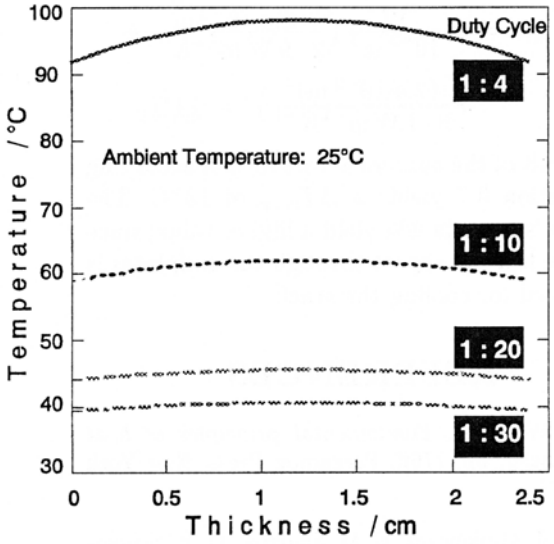

FIGURE 0.10: Distribution of maximum temperature across the 30 V/65 F starter capacitor at different ambient temperatures and duty cycles. Thickness of the stack 2.5 cm.

With respect to the design of supercapacitors in the near future, constructive efforts will aim at improving heat transmission and thermal radiation. In order to make the integration of cost-effective components feasible, external cooling must be avoided.

ENGINEERING FORMULA

A simple formula was found which yields a rough estimate of the total heat output and the maximum temperature in laboratory supercacitors. It can be used to complement complex numerical

modelling calculations. As long as only the heat transport through the endplates of the capacitor is considered (i.e. $\alpha_{stack} \to 0$), the maximum temperature difference can be calculated as:

$$\boxed{\Delta T_{max} = \frac{\dot{Q}}{V}\left(\frac{d_{stack}}{2\alpha_{end}} + \frac{d_{stack}^2}{8\lambda_z}\right)}. \qquad (0\text{-}9)$$

Here, the heat transfer coefficient of the capacitor in z-direction is $\lambda_z \approx 1.0$. The heat transfer coefficientr at the phase boundary between the endplates and the ambient air is $\alpha_{end} \approx 7 \ldots 10$ $\mathrm{W\,K^{-1}m^{-2}}$. d_{stack} is the thickness of the stack (without endplates).

Example. For a 2 ℓ capacitor with an internal resistance of $R_i = 0.04\ \Omega$ which is discharged at 100 A, $\dot{Q}/V = 200\,\mathrm{W}/\ell$. Assuming the duty cycle during extended operation is 1 : 40 (i.e. the capacitor is discharged for 1 s, and charged for 40 s) the volume specific thermal output will be 10 W/ℓ. With the heat transfer coefficient taken from Figure 0.8 being $\alpha = 9\ \mathrm{W/m^2K}$, the maximum temperature in a stack of 2.4 cm thickness will be:

$$\Delta T_{max} = 10\,\frac{\mathrm{W}}{10^{-3}\,\mathrm{m}^3}\left(\frac{2.4\cdot10^{-2}\,\mathrm{m}}{2\cdot 9\,\mathrm{W\,m^{-2}K^{-1}}} + \right.$$
$$\left. + \frac{(2.4\cdot10^{-2}\,\mathrm{m})^2}{8\cdot 1\,\mathrm{W\,m^{-1}K^{-1}}}\right) = \underline{\underline{14\,^\circ\mathrm{C}}}.$$

The result of the numerical calculation according to equation 0-7 yields a ΔT_{max} of 13 °C. The engineer's formula will yield a higher value, since only the heat transport through the endplates is considered for cooling the stack.

REFERENCES

[1] S. Whitaker, *Fundamental principles of heat transfer*, pp. 176ff, Pergamon Press, New York 1977.

[2] W. J. Minkowycz, E. M. Sparrow, G. E. Schneider, R. H. Pletcher, *Handbook of numerical heat transfer*, Wiley Interscience, New York 1988.

[3] W. H. Press, B. P. Flannery, S. H. Teukolsky, W. T. Vetterling, *Numerical Recipes in Pascal*, pp. 669ff, Cambridge University Press, 1990.

[4] *VDI-Wärmeatlas*, pp. Fa 1ff., VDI-Verlag GmbH, Düsseldorf 1984.

[5] Gröber, Erk, Grigull, *Wärmeübertragung*, pp. 18–24, Springer, Berlin 1963.